Published in final edited form as:
Nature. 2021 September 01; 597(7877): 533–538. doi:10.1038/s41586-021-03891-8.

Bioaccumulation of therapeutic drugs by human gut bacteria

Martina Klünemann[#1,4], **Sergej Andrejev**[#1], **Sonja Blasche**[#1,17], **Andre Mateus**[#1], **Prasad Phapale**[1], **Saravanan Devendran**[1], **Johanna Vappiani**[3], **Bernd Simon**[1], **Timothy Scott**[2], **Eleni Kafkia**[17], **Dimitrios Konstantinidis**[1], **Katharina Zirngibl**[1,17], **Eleonora Mastrorilli**[1], **Manuel Banzhaf**[1,5], **Marie-Therese Mackmull**[1,6], **Felix Hövelmann**[1], **Leo Nesme**[1,7], **Ana Rita Brochado**[1,8], **Lisa Maier**[1,9], **Thomas Bock**[1,10], **Vinita Periwal**[1,17], **Manjeet Kumar**[1], **Yongkyu Kim**[1], **Melanie Tramontano**[1,11], **Carsten Schultz**[1], **Martin Beck**[1], **Janosch Hennig**[1], **Michael Zimmermann**[1], **Daniel C. Sévin**[3], **Filipe Cabreiro**[2,12,13], **Mikhail M. Savitski**[1], **Peer Bork**[1,14,15,16,*], **Athanasios Typas**[1,*], **Kiran R. Patil**[1,17,*]

[1]European Molecular Biology Laboratory, Heidelberg, Germany

[2]Institute of Structural and Molecular Biology, University College London, UK

[3]Cellzome, GlaxoSmithKline R&D, Heidelberg, Germany

[12]Institute of Clinical Sciences, Imperial College London, UK

[14]Max Delbrück Centre for Molecular Medicine, Berlin, Germany

[15]Yonsei Frontier Lab (YFL), Yonsei University, Seoul 03722, South Korea

[16]Department of Bioinformatics, Biocenter, University of Würzburg, Würzburg, Germany

[*]**Correspondence and requests for materials** should be addressed to P.B., A.T. or K.R.P. bork@embl.de, typas@embl.de, kp533@cam.ac.uk.
[4]Present address: Evonik Operations GmbH, Essen, Germany
[5]Present address: School of Biosciences, University of Birmingham, UK
[6]Present address: ETH Zürich, Switzerland.
[7]Present address: Molecular Health GmbH, Heidelberg, Germany
[8]Present address: University of Würzburg, Germany
[9]Present address: University of Tübingen, Germany
[10]Present address: Biozentrum, University of Basel, Switzerland
[11]Presen address: German Cancer Research Center, Heidelberg, Germany
[13]Present address: CECAD, University of Cologne, Germany

Author contributions

M.K., P.B., A.T. and K.R.P. conceived the study. M.K., S.A., A.T. and K.R.P. planned the overall experiments. S.A. performed the overall data analysis. K.Z. and V.P. performed the drug clustering. M.K. carried out the interaction screen, large-volume validation, and UPLC data analysis. A.R.B., L.M., M.T. and M. Banzhaf. assisted with the screen set-up. F.H. and C.S. designed and synthesized the clickable drug. M.K., M.M., and T.B. performed the click-chemistry proteomics experiments. M.B. designed and supervised the click-chemistry proteomics analysis. A.M. and M.M.S. planned the TPP experiments. S.B. and A.M. performed the TPP experiments. A.M., M.M.S. and S.A. analyzed the TPP data. J.V. and D.C.S. performed the FIA-MS experiments and data analysis. S.B. performed the bacterial culturing experiments, and P.P. performed the LC-MS analysis for drug measurements. M.K. and P.P. performed the secreted metabolite LC-MS analysis in buffer. M.K. and S.B. prepared the samples for, and B.S., L.N. and J.H. performed the NMR analysis. M.K. and D.K. performed growth assays and sample preparation for cross-fed metabolite analysis. S.B. performed growth assays and sample preparation for secreted metabolite analysis in GMM. S.D., E.M., E.K., and M.Z. performed the HILIC-MS/MS analysis. K.Z. analyzed the cross-feeding metabolomics data. M.Kumar performed the motif analysis. M.K. performed the community assembly experiments and Y.K. analyzed the 16S data. T.S. and F.C. performed the C. elegans experiments and data analysis, D.K. measured drug concentrations. M.K and K.R.P. wrote the paper.

Competing interests

M.K., S.A., L.M., M.T., P.B., A.T. and K.R.P. are inventors in a patent application based on the findings reported in this study (US patent application number 16966322). S.B., A.M., P.P., S.D., J.V., B.S., T.S., E.K., D.K., K.Z., E.M., M. Banzhaf, M.M., F.H., L.N., A.R.B., T.B., V.P., M. Kumar, C.S., M. Beck, J.H., M.Z., D.C.S., F.C., and M.M.S. declare no competing interests.

Europe PMC Funders Author Manuscripts

[17]Medical Research Council Toxicology Unit, Cambridge, United Kingdom

[#] These authors contributed equally to this work.

Abstract

Bacteria in the gut can modulate the availability and efficacy of therapeutic drugs. Yet, the systematic mapping of the respective interactions has only started recently[1] and the main underlying mechanism proposed is chemical transformation of drugs by microbes (biotransformation). Here, we investigated the depletion of 15 structurally diverse drugs by 25 representative gut bacterial strains. This revealed 70 bacteria-drug interactions, 29 of which had not been reported before. Over half of the new interactions can be ascribed to bioaccumulation, that is bacteria storing the drug intracellularly without chemically modifying it, and in most cases without their growth being affected. As a case in point, we studied the molecular basis of bioaccumulation of the widely used antidepressant duloxetine by using click-chemistry, thermal proteome profiling and metabolomics. We find that duloxetine binds to several metabolic enzymes and changes metabolite secretion of the respective bacteria. When tested in a defined microbial community of accumulators and non-accumulators, duloxetine markedly altered the community composition through metabolic cross-feeding. We further validated our findings in an animal model, showing that bioaccumulating bacteria attenuate the behavioral response of *Caenorhabditis elegans* to duloxetine. Taken together, bioaccumulation by gut bacteria may be a common mechanism that alters drug availability and bacterial metabolism, with implications for microbiota composition, pharmacokinetics, side effects and drug responses, likely in an individual manner.

Therapeutic drugs can have a strong impact on the gut microbiome and vice versa[2–5]. The underlying drug-bacteria interactions can reduce microbial fitness[6] or alter the drug availability through biotransformation[7–14]. The latter can have either a positive or a negative impact on drug activity and efficacy. While drugs like lovastatin and sulfasalazine are chemically transformed by gut bacteria into their active forms, bacterial metabolism can inactivate drugs such as digoxin[15,16], or cause toxic effects as in the case of irinotecan[17]. Furthering the diversity of susceptible drugs, over one hundred molecules were recently reported to be chemically modified by gut bacteria[1]. Yet, the mechanistic view on these interactions is largely confined to drug biotransformation[12,13].

Drug accumulation without metabolization

To expand the knowledge of bacterial effect on drug availability, we systematically profiled interactions between 15 human-targeted drugs and 25 representative human gut bacterial strains (21 species; with additional subspecies or conspecific strains of *Bifidobacterium longum*, *Escherichia coli* and *Bacteroides uniformis*) (Supplementary Table 1). The bacterial species were selected to cover a broad phylogenetic and metabolic diversity representative of the healthy microbiota[18] (Supplementary Fig. 1a, Supplementary Table 1). On the drug side, 12 orally administered small molecule drugs (MW<500 Da), amenable to UPLC-UV-based quantification, were selected to span diverse chemistry, indication areas and side-effect profiles (Supplementary Fig. 1b-e, Supplementary Table 2). Three additional drugs were included as controls: digoxin with its highly specific interaction with *Eggerthella lenta*[16], and, metronidazole and sulfasalazine, which are metabolized by several gut bacteria[19–21].

The resulting 375 bacteria-drug pairs were tested for drug depletion in two independent screens (Methods). The bacteria were grown in Gut Microbiome Medium (GMM)[22] and the initial drug concentration was set to 50 μM, which, while being close to the estimated colon concentration range for many drugs[6], allowed reliable measurement of concentration changes. For each pair, depletion of the drug from the culture supernatant was measured using UPLC-UV analysis after 48 h of anaerobic growth (Methods). Validating the assay, the control drugs metronidazole and sulfasalazine were depleted by most of the strains, and digoxin was depleted exclusively by *E. lenta*[16]. An FDR-corrected p-value cut-off of 0.05 and a threshold of 30 % depletion were used for calling interactions (based on the digoxin depletion by *E. lenta* as a case with established *in vivo* relevance, Supplementary Table 3). All new interactions found in the screen were again evaluated in independent assays performed in larger volume cultures (Supplementary Fig. 2). The interactions with statistical support in the second assay as well as those with the support from previous studies revealed a network spanning all of the tested strains and 66% of the tested drugs (10 of 15) (Fig. 1). Twenty-nine of these interactions (18 species and 7 drugs) have not, to our knowledge, been previously reported.

To track the fate of the depleted drugs, we measured post-growth drug concentrations in culture supernatants as well as in total culture extracts including cells (Methods). Comparison between the two revealed 17 cases wherein the drug was depleted in the supernatant but could be recovered from the total culture (Supplementary Table 3). This implied an accumulation rather than a chemical transformation of the respective drugs by bacteria. This was surprising as until now, biotransformation has been recognized as the main mode of drug depletion by bacteria[1,12–14].

As many as 17 of the 29 newly identified interactions (14 species and 4 drugs) were bioaccumulation events, that is storage of the drug by bacteria without modifying it. The remaining 12 interactions (8 species and 5 drugs) likely represent biotransformation events. Two of the 5 drugs, levamisole and ezetimibe, have indeed been shown to be chemically modified by other gut bacteria[1,23]. Among the bioaccumulated drugs, the antidepressant duloxetine and the antidiabetic rosiglitazone were exclusively bioaccumulated, each in a number of different species (Fig. 1). Yet, biodegradation and bioaccumulation interactions were not mutually exclusive. Montelukast (used in asthma treatment) and roflumilast (used against chronic obstructive pulmonary disease) were bioaccumulated by some and degraded by other bacteria. On the bacterial side, all strains but *Fusobacterium nucleatum* showed both interaction types. The conspecific strains of *B. uniformis* and *E. coli* showed no overlap in their interactions, except for those with the broadly interacting control drugs sulfasalazine and metronidazole. As individuals typically harbor different strains[24], it is likely that the prevalence of bioaccumulation interactions is higher than reported here.

As many human-targeted drugs have been shown to impact the growth of gut bacteria[6], we examined whether the identified bacteria-drug interactions resulted also in altered growth. While over 30, mostly inhibitory, drug-bacteria interactions were detected, interactions involving both modified growth and altered drug concentration were only 3 (excluding the control drugs sulfasalazine and metronidazole) (Fig. 1, Supplementary Table 3). Thus, bacteria-drug and drug-bacteria interactions appear to be largely independent.

To attest the bioaccumulation nature of the identified bacteria-drug interactions, we used two additional analytical methods, NMR spectroscopy and LC-MS (Methods). As a case in point, we focused on duloxetine, a widely used antidepressant that was found to be bioaccumulated by eight species. NMR spectroscopy allowed us to unambiguously detect duloxetine and confirmed that the four selected strains (*S. salivarius*, *B. uniformis*, *E. coli* IAI1 and *E. coli* ED1a) depleted it from the media without biotransforming it (Fig. 2a-b, Supplementary Fig. 3-4). These assays were performed using cells suspended in PBS buffer to circumvent the complexity of the GMM medium. While only one of the two *E. coli* strains (IAI1) bioaccumulated to an appreciable extent in GMM, both strains extensively depleted duloxetine under these nutrient-deprived conditions. The LC-MS analysis in the complex GMM media also confirmed bioaccumulation by *C. saccharolyticum* and *E. coli* IAI1 at a range of concentrations between 30 to 70 μM (Fig. 2c, Supplementary Fig. 5).

Bioaccumulation impacts cell metabolism

While biotransformation can be attributed to metabolic enzymes[7], drug bioaccumulation is mechanistically more difficult to picture. Bioaccumulation of small molecules that are not designed to target microbes has been observed before in other ecosystems, such as in soil or activated sludge bioreactors[25–28]. To investigate the molecular basis of drug bioaccumulation by gut bacteria, we set out to identify protein targets of duloxetine in bioaccumulating strains. We started by constructing an alkynated, ‘clickable’, version of the molecule to use as a bait (Supplementary Fig. 6a, Methods). Fifty-five proteins, mostly metabolic enzymes, were enriched in the pull-down from *C. saccharolyticum* lysate compared to the drug-treated control (log2(Fc)≥2, FDR adjusted p <0.1; Supplementary Fig. 6b, Supplementary Table 4). Although these results strongly indicate duloxetine binding to specific protein targets, the use of a structurally modified version of the molecule precludes direct conclusion. We therefore additionally used thermal proteome profiling (TPP)[29,30] to systematically identify proteins undergoing structural changes (stabilization/destabilization with respect to heat induced unfolding) upon exposure to unmodified duloxetine. Supporting the click-chemistry based assays, TPP revealed several metabolic enzymes among the proteins structurally responding to duloxetine (Supplementary Table 5). Affected pathways include amino acid metabolism, purine and pyrimidine biosynthesis, and the pentose-phosphate pathway that provides precursors for nucleotide biosynthesis (Fig. 2d, Supplementary Table 5-6). Many of these proteins belong to the NADH:ubiquinone dehydrogenase complex, and contain a Rossmann fold associated with nucleotide binding (Supplementary Table 5).

The click-chemistry and TPP results suggest protein binding as a contributing factor to duloxetine bioaccumulation. This raised the question of why the two *E. coli* strains exhibited different degree of duloxetine bioaccumulation in GMM. We compared the two *E. coli* strains in two different TPP assays wherein the drug was added either to lysed or to intact cells. While the TPP in cell lysates would uncover proteins (de-)stabilized due to direct duloxetine binding, the intact cell TPP would additionally capture, under the *in vivo* conditions, the changes in the cellular response (changes in protein interactions and activity). In the intact cell assay, the bioaccumulating IAI1 strain had almost two-fold more drug-responding proteins than the non-bioaccumulating ED1a strain (388 vs 222 proteins), and

stronger overall changes in thermal stability (Fig. 2e, Supplementary Table 5). In agreement with duloxetine changing the cellular physiology more drastically in the bioaccumulating strains, the IAI1 strain also showed a more pronounced response in differentially expressed proteins (Supplementary Fig. 6c-d, Supplementary Table 7). In contrast, the two strains exhibited very similar profiles in lysate-based TPP wherein the lack of cell envelope allows the drug to reach all intracellular proteins (397 vs 412 proteins; Fig. 2e). It is thus likely that the strain-specificity of bioaccumulation is due to differences in uptake and efflux systems, analogous to the transporter-dependent specificity observed in drug-drug interactions[31].

The binding of duloxetine to metabolic enzymes suggests altered metabolism in bioaccumulators. To test this, we used two complementary metabolomics platforms, flow-injection MS and HILIC-MS/MS (Methods), to profile the impact of duloxetine treatment on small molecule secretion by six bacterial strains (four bioaccumulating and two non-bioaccumulating). Four strains, three bioaccumulating (*C. saccharolyticum*, *L. plantarum*, and *E. coli* IAI1) and one non-bioaccumulating (*L. lactis*), showed a significant shift in their exo-metabolome pattern upon drug treatment in GMM ($p < 0.05$, two-sample Hotelling's t-squared test; Fig 2f, Supplementary Fig. 7, Supplementary Table 8-9, 12A). *C. saccharolyticum* was particularly notable with the drug-induced shift in its exo-metabolome being comparable to that of interspecies differences (Fig 2f). Furthermore, the drug response was concentration-dependent (Fig. 2g, Supplementary Fig. 7b,c), and no effect was observed for the non-bioaccumulated roflumilast (Supplementary Fig. 8a). The concentration-dependent response to duloxetine was further validated with a subset of 71 metabolites, whose chemical identity was putatively assigned – with two metabolites confirmed using chemical standards – using tandem mass-spectrometry (Methods, Supplementary Fig. 8b, Supplementary Table 10). *C. saccharolyticum* showed a strong metabolic response to duloxetine also when probed in nutrient-deprived PBS buffer (Supplementary Table 11, 12B, Fig. 2d, Supplementary Fig. 6e-h). Together, the proteomic and the metabolomic data show binding of duloxetine to abundant metabolic enzymes, supporting its intracellular storage.

Bioaccumulation induces cross-feeding

Metabolic interactions are fundamental in shaping the composition of gut microbial communities[32,33]. We therefore asked whether metabolic changes associated with bioaccumulation can impact community composition. To address this, we assembled stable communities of five gut bacterial species (*Bacteroides thetaiotaomicron*, *Eubacterium rectale*, *Lactobacillus gasseri*, *Ruminococcus torques*, and *Streptococcus salivarius*) in the presence and the absence of duloxetine. One of the five species is a duloxetine bioaccumulator (*S. salivarius*) and another is directly inhibited by duloxetine (*E. rectale*). The five species were co-inoculated in GMM and subsequently transferred to fresh medium every 48 hours. The presence of duloxetine markedly shifted the community composition, allowing *E. rectale* to increase its abundance over 100-fold as compared to that without the drug (Fig. 3a, Supplementary Fig. 9a-b). This was surprising since *E. rectale* is the most sensitive to duloxetine among the five used species (Fig. 3b, Supplementary Table 13). Consistent with *S. salivarius* being bioaccumulator, duloxetine was depleted in the community supernatant (circa 15% decrease; relative abundance *S. salivarius* circa 20%)

(Supplementary Fig. 9c). Although decreased duloxetine concentration could protect *E. rectale* in the community, its bloom in the presence of duloxetine would require growth-promoting interactions.

We hypothesized that the changed metabolite secretion by *S. salivarius* in response to duloxetine could boost *E. rectale*. Supporting this, the spent medium from *S. salivarius* grown in the presence of the drug improved the growth of *E. rectale* (Fig. 3c). Untargeted metabolomics data from both flow-injection MS and HILIC LC-MS/MS further supported the cross-feeding hypothesis. Accordingly, several metabolites were found to be accumulated during *S. salivarius* cultivation and subsequently depleted during *E. rectale* growth (Fig. 3d, Supplementary Fig. 9d, Supplementary Table 14-15). Five of these metabolites were putatively annotated, and two, linolenic acid and glycocholic acid, were confirmed using analytical standards (Methods). The changes in nucleotide-related metabolites, such as uridine 5'-diphosphate, are in line with the proteins and metabolites affected by duloxetine (Fig. 2d), and that with the fastidious nature of *E. rectale*[18]. Thus, human-targeted drugs can modulate gut microbial communities, not only through direct inhibition[2,6], but also by creating cross-feeding opportunities.

Bioaccumulation affects host response

We next investigated the effect of duloxetine bioaccumulation on host response using *Caenorhabditis elegans* as a model system. Duloxetine, as a serotonin-norepinephrine reuptake inhibitor, regulates the behavior (muscular movement) of *C. elegans* in a concentration-dependent manner (Supplementary Fig. 9e). We examined animal movement as behavioral readout in the presence of a bioaccumulating species (*E. coli* IAI1) as part of the *C. elegans* growth medium. As a closely related control, we used the strain *E. coli* ED1a that did not bioaccumulate in complex growth medium. Indeed, only the duloxetine-bioaccumulating strain IAI1 attenuated the effect of duloxetine on the host (Fig. 3e). Although the *C. elegans* gut is colonised by facultative anaerobes and obligate aerobes and is thus likely to be aerobic[34], our results agree well with the bioaccumulation observed in the anaerobic culture experiments. Further investigation of the microbiome-duloxetine-host interaction in other model systems or in a clinical setting is thus warranted.

Discussion

Our results uncover two ways by which therapeutic effects of host-targeted drugs could be modulated due to bioaccumulation by gut bacteria: a primary effect due to reduced drug availability, and a secondary effect due to changed metabolite secretion. The latter can lead to changes in community composition, which is associated with side-effects or even the mode of action of some drugs[2,35,36]. For our case-in-point drug duloxetine, gut bacterial interactions are indeed implicated in side-effects like weight gain, and also in its mode of action[37–39]. In a broader perspective, our study calls for a systematic mapping of reciprocal interactions between drugs and gut bacteria – drugs impacting microbes and microbes biotransforming or bioaccumulating drugs – both individually for measuring direct effects, and in communities for estimating secondary effects.

Methods

Growth conditions

Unless otherwise indicated, all bacteria were grown as liquid cultures in Gut Microbiota Medium (GMM)[22]. Cultivations were carried out in a Vinyl Anaerobic Chamber (COY, USA) at 37 °C with oxygen below 20 ppm, 15% carbon dioxide and 1.8-2% hydrogen. Main gas in the anaerobic chamber was nitrogen. All experimental cultures were started from the second passage culture after inoculation from a glycerol or DMSO stock. All media, buffer, glass and plasticware used in the study were exposed to the anaerobic conditions at least 12 h prior to their usage.

Bacteria-drug interaction screen

For all drugs, a fixed concentration of 50 μM was used, which is within the colon concentration range estimated for many drugs[6]. Triplicates for each bacterium-drug interaction and a single bacteria-free control were screened per plate and drug. Bacteria-free controls from multiple plates within a batch were pooled together (at least 4 per drug, median = 17) for comparison with the corresponding treated samples. Wilcoxon's rank sum test and a p-value cut-off 0.05 (after FDR correction) was used to assess statistical significance. The screen was carried out under anaerobic conditions in 96-well plates (Nunclon Delta Surface 163320, NUNC) with 150 μl GMM as the growth medium sealed with a Breathe-Easy® sealing membrane (Z380059, Sigma-Aldrich). Plates containing 100 μl of the medium and 75 μM of the drug were prepared beforehand, stored at -20 °C and used as needed. Frozen plates were introduced into the anaerobic chamber the evening before inoculation. Wells were inoculated with 50 μl of a second passage culture to reach starting OD578 of 0.01. Growth was monitored by measuring optical densities at 578 nm using an Eon Microplate Spectrophotometer (BioTek) approximately every 2 h for the first 10 h, and then approximately every 6 h. After 48 h, plates were removed from the anaerobic chamber and the bacteria were spun down (4000 rpm, 10 min) to harvest the supernatant. 100 μl of it was extracted in 300 μl ice cold acetonitrile:methanol (Biosolve, ULC/MS grade) in 500 μl polypropylene plates (Corning Costar 3957) to remove compounds interfering with liquid chromatography. Plates were closed with a lid (Corning, storage mat 3080) and after shaking and 15 minutes incubation at 4 °C, samples were centrifuged at 4000 rpm for 10 min at 4 °C and 300 μl of the supernatant were transferred to a new plate (Corning Costar 3362). All liquid handling outside of the anaerobic chamber was done using a ducted liquid handling robot (FXp, Biomek). Sample plates were then left overnight in a chemical hood to evaporate the organic phase, before being stored at -20 °C. For estimating the drug concentration in the samples with the UPLC, samples were reconstituted in 50 μl 20% acetonitrile solution containing 250 μM caffeine (Sigma) as an internal standard.

Screen validation and bioaccumulation detection

Bacteria from second passage culture were inoculated at starting OD578 of 0.01 in 1 mL GMM containing 50 μM drug of interest in 2 mL eppendorf tubes and incubated for 48 h while shaking. After the growth, the cultures were removed from the anaerobic chamber. 800 μl of each sample was transferred to a new eppendorf tube, while the remaining

200 µl were directly extracted by adding 600 µl ice-cold acetonitrile:methanol solution and incubated for 15 min at 4 °C. For supernatant extraction, the transferred culture was centrifuged for 5 min at 14000 rpm to pellet the bacteria, and 200 µl of the bacteria-free supernatant was extracted in a new eppendorf tube, respectively. After the 15 min 4 °C incubation period, all samples were centrifuged for 10 min, 14.000 rpm at 4 °C and 700 µl of the supernatant was transferred to a new eppendorf tube. Samples were dried for 5-7 h at 30 °C in a speedvac (Eppendorf Vacuum Concentrator Plus, V-AL mode) and stored at -20 °C until used for UPLC measurement. Samples were reconstituted in 116 µl 20% acetonitrile containing 250 µM caffeine. All interactions and controls were tested in triplicates.

UPLC analysis

Liquid chromatography analyses were run on a Waters Acquity UPLC H-Class instrument with a PDA detector and a quaternary solvent system. Each run was circa 5 minutes long, with a flow rate of 0.5 ml/min and run on a CSH C18 column (Waters, Part number 186005297; 130Å, 1.7 µm, 2.1 mm X 100 mm) in reverse mode. The column was heated to 40°C and samples kept at 6 °C. All methods used 50% acetonitrile (Biosolve, ULC grade) as washing buffer, and 50% methanol (Biosolve, ULC grade) as purging buffer. As organic mobile phase, acetonitrile was used. The assay used two additional buffers besides water as hydrophilic mobile phase: 5 mM formic acid (Biosolve, ULC grade) of pH 3.2 and 5 mM ammonium formate (Ammonium hydroxide, ACS grade, Sigma) with pH adjusted to 8.3 using formic acid. Supplementary Table 16 lists the five different chromatographic methods established for the different drugs. During the method development, we checked for the absence of interference from bacterial or growth medium metabolites by running bacteria-only and media samples. Carrier treated bacterial cultures were also included in the screen and the corresponding UPLC results were inspected for the absence of any peaks that could overlap with the drug peak (Supplementary Fig. 1).

NMR analysis

Bacteria were grown in GMM for one or two days (depending on the growth rate of the strain) at 37°C without shaking in an anaerobic chamber. The cells were harvested by centrifugation and washed twice with PBS, pH 6.5 buffer under anaerobic conditions and then resuspended at a final OD of 3.75 in PBS containing duloxetine or an equivalent amount of DMSO (standard DMSO or deuterated DMSO) prior incubation for 4 hours at 37°C in an anaerobic chamber. Samples were then centrifuged for 2 min at 8000 rpm to separate cells and supernatant. The supernatant was directly used for NMR analysis (540 µl). For extracting the drug from cell pellets, the pellet was resuspended in 200 µl methanol, before addition of 600 µl deuterated DMSO and 0.4 g acid-washed glass beads. Bead beating was done for 1 min at 4°C at 6.5 m/s. 540 µl of extract without beads were used for NMR analysis. The duloxetine concentration was quantified by comparing the peak integrals of isolated peaks to the signals of a reference spectrum of pure duloxetine dissolved in the corresponding deuterated solvent and the chemical shifts were referenced to the residual proton signal of the solvent in this spectrum. 1D proton NMR spectra with water pre-saturation were measured for all samples at 298 K on a Bruker Avance III 700 MHz spectrometer equipped with a triple resonance room temperature probe head. Each spectrum

was acquired with 128 scans, using an interscan delay of 6.2 s (2.2 s acquisition time) and was processed with Topspin 3.5 (Bruker).

LC-MS/MS duloxetine measurements (Reverse phase LC-MS/MS, Orbitrap)

LC-MS/MS analysis was performed on a Vanquish UPLC system coupled with Q-Exactive plus HRMS (Thermo Fisher Scientific, MA, USA). The injection volume was 2µL and the separation was carried out on Waters ACQUITY UPLC HSS T3 column (2.1 x 100 mm, 1.8 µm; Waters UK) at the flow rate of 0.3 ml/min and maintained at 40 °C. The mobile phase consisted of solvent A (0.1 % formic acid in water) and solvent B (0.1 % formic acid in methanol) with a 10 min gradient, starting at 10% of solvent B for 2 min, which was ramped up to 90% for next 2 min and then hold for 2 min followed by 4 min of equilibration to the starting condition (10% of solvent B). The analytes were detected with HRMS full scan at the mass resolving power R=35000 in a mass range of 60-900 *m/z*. For identification of analytes; the data-dependent tandem (MS/MS) scans were obtained along with full scans using higher-energy collisional dissociation (HCD) with normalized collision energies of 30, 35 and 40 units (at R=17500), which were then compared with MS/MS spectra obtained from authentic standards. The MS parameters in the Tune software (Thermo Scientific) were set as: ESI positive voltage of 4 kV, sheath gas 30 and auxiliary gas 5 units, S-Lens 65 eV, capillary temperature 320 °C and vaporization temperature of auxiliary gas was 250 °C. The data analysis and quantification of drugs was performed using the Xcalibur Quan Browser software (Thermo Scientific). Three internal standards were used: fluoxetine, sulfamethizole and sulfamethazine. In addition, to account for the complex matrix effects, drug standards were prepared by adding the drug to the *C. saccharolyticum* supernatants or cell lysates and extracting from these in acetonitrile:methanol in the same manner as for the samples. Solvent blanks (acetonitrile:methanol) and media-only controls (incubated as the samples) were run intermittently to ensure that there was no drug carry-over from the system.

Click-chemistry based identification of duloxetine binding proteins

Bacterial suspensions of *C. saccharolyticum* (1 ml, anaerobic conditions) were lysed by bead disruption and additional sonication at 4 °C (two times at 75% amplitude/0.5 s cycle for one minute, Hielscher sonicator). Supernatant after centrifugation at 20000 x g at 4 °C for 10 minutes containing protein lysate was recovered and protease inhibitors (aprotinin 10 µg/mL, leupeptin 5 µg/mL) were added. For all duloxetine-protein pull-downs, Strep-Tactin® Sepharose® 50% suspension (#2-1201-025, IBA) was used. For each sample, 400 µl Strep-Tactin Sepharose (50% suspension) was pre-washed three times using 400 µl PBS (pH=7) at room temperature. Beads were bound to duloxetine before addition of the protein lysate by resuspension in 400 µl PBS containing 50 µM duloxetine (control) or 50 µM duloxetine linked to desthiobiotin (for pull-down) on a rotating wheel at room temperature for 30 minutes. Unbound drug was removed by three PBS wash cycles (400 µl each). Protein lysates were incubated with drug-bound beads on a rotating wheel at 4 °C overnight. Unbound proteins were removed by washing the beads with cold PBS. Bound proteins were recovered by competitive elution using PBS containing 5 mM Biotin. After an SDS gel using stain-free SDS-PAGE imaging technology (BioRad) showed protein integrity, samples were further processed for mass spectrometry-based protein identification. The pull down was conducted in quadruplicates for each treated and control sample.

For the identification of recovered proteins by mass spectrometry, protein eluates were rebuffered into 4 M urea / 0.2% rapigest (final concentration) and sonicated in a vial tweeter (Hielscher) for two times 30 seconds (100% / 0.5 seconds cycle). Disulfide bridges between cysteines were disrupted by reduction with 10 mM DTT at 37 °C for 30 minutes. Following that, free cysteines were alkylated using 15 mM iodoacetamide at room temperature in the dark for 30 minutes. Protein digestion was performed using 1:100 (w/w) Lys-C endoproteinase (Wako Chemicals GmbH, Germany) at 37 °C for 4 h and then finalized (after the urea concentration was diluted to 1.6 M) with 1:50 (w/w) trypsin (Promega GmbH, Germany) at 37 °C overnight. Rapigest was cleaved by acidification below pH=3 using 10% (v/v) TFA at room temperature for 30 minutes and removed by desalting of the peptide mixture using C18 spin columns (Harvard Apparatus, USA) according to the manufacturer's procedures. Desalted peptides were vacuum dried and stored at -20 °C until further use. These samples were analyzed using a nanoAcquity UPLC system (Waters GmbH) connected online to a LTQ-Orbitrap Velos Pro instrument (Thermo Fisher Scientific GmbH). Peptides were separated on a BEH300 C18 (75 μm x 250 mm, 1.7 μm) nanoAcquity UPLC column (Waters GmbH) using a stepwise 90 min gradient between 3 and 85% (v/v) ACN in 0.1% (v/v) FA. Data acquisition was performed by collision-induced dissociation using a TOP-20 strategy with standard parameters. For the quantitative label-free analysis, raw files from the Orbitrap were analyzed using MaxQuant (version 1.5.3.28) [41]. MS/MS spectra were searched against the *Clostridium saccharolyticum* (strain ATCC 35040 / DSM 2544 / NRCC 2533 / WM1) entries of the Uniprot KB (database release 2016_04, 7212 entries) using the Andromeda search engine[42]. The search criteria were set as follows: full tryptic specificity was required (cleavage after lysine or arginine residues, unless followed by proline); 2 missed cleavages were allowed; carbamidomethylation (C) was set as fixed modification; oxidation (M) and acetylation (protein N-term) were applied as variable modifications, if applicable; mass tolerance of 20 ppm (precursor) and 0.5 Da (fragments). The reversed sequences of the target database were used as decoy database. Peptide and protein hits were filtered at a false discovery rate of 1% using a target-decoy strategy[43]. Additionally, only proteins identified by at least 2 unique peptides were retained. Only proteins identified in at least 2 replicates were considered when comparing protein abundances between control and drug treatment.

To reduce technical variation, data was quantile-normalized using the preprocessCore library[44]. Protein differential expression was evaluated using the limma package. Differences in protein abundances were statistically determined using the Student's t-test moderated by Benjamini-Hochberg's method[45] at alpha level of 0.05. Significantly regulated proteins were defined by a cutoff of log2 fold change ≥ 2 and $p \leq 0.1$. Presented values are reached after imputing for not-missing-at-random from controls and correcting for an overall higher intensity in test samples in comparison to control samples. For gene ontology term and pathway enrichment analysis, significantly changed proteins were annotated using Blast2GO[46] with default parameters using the NCBI blast search. GO term enrichment was done within Blast2GO and significantly enriched (FDR corrected $p<0.05$) most specific GO terms were listed. For KEGG pathway enrichment analysis EC numbers from Blast2Go annotation were extracted and the EC2KEGG tool[47] was used to annotate respective species specific KEGG pathways and perform enrichment analysis ($p < 0.05$).

2D-Thermal Proteome Profiling and protein expression analysis

Thermal proteome profiling was performed as previously described [29,48]. Briefly, cells were grown anaerobically at 37 °C for 48 hours. Cells were then washed twice and OD adjusted to 5. For whole cell experiments, duloxetine was then added at five different concentrations and incubated for 30 min. For lysate experiments, cells were disrupted with five freeze-thaw cycles prior to duloxetine treatment. Aliquots of treated cells or lysates were then heated for 3 min to ten different temperatures in a PCR machine (Agilent SureCycler 8800). After cell lysis, protein aggregates were removed and the remaining soluble proteins were collected.

For full proteome quantification, cells were inoculated at OD^{578} 0.01 and duloxetine was added at five different concentrations. Cells were grown anaerobically for 48 h, washed twice with PBS and lysed as previously described [48].

Proteins from these experiments were digested according to a modified SP3 protocol[49,50], as previously described[48]. Peptides were labeled with TMT10plex (Thermo Fisher Scientific), fractionated onto six fractions under high pH conditions and analyzed with liquid chromatography coupled to tandem mass spectrometry, as previously described[48]. Protein identification and quantification was performed using IsobarQuant[30] and Mascot 2.4 (Matrix Science) against Uniprot Proteome (ID: UP000000625 for *E. coli* IAI1, UP000000748 for *E. coli* ED1a, and UP000001662 for *C. saccharolyticum*). Data was analyzed with the TPP package for R[30].

Secreted metabolite analysis (Reverse phase LC-MS/MS, Orbitrap)

Bacterial cells from a 20mL overnight culture were washed for use in resting cell and lysate assays as described below. Duloxetine concentration used was 1 mM and all interactions were tested in triplicates. For the resting cell assay, bacteria were reconstituted in 3.6 mL PBS, pH 6.5 containing 1 mM MgCl2, sample volume was 600 µl. For the lysate assay, bacteria were reconstituted in 1 mL PBS, lysed, and then 360 µl of the recovered lysate diluted with 1080 µl PBS, thus final sample volume for each replicate (6 in total; 3 drug and 3 control) was 240 µl. Resting cells were incubated for 2 h and lysates for 30 min with duloxetine or with DMSO as control. As another control, buffer with duloxetine was incubated for the respective time in the respective sample volume. Cells/lysate was centrifuged (14.000rpm, 10min, 4°C) and only the supernatant was extracted (450 µl for resting cells, and 187.5 µl in case of lysates) in ice-cold 1:1 methanol:acetonitrile containing 10µM amitriptyline as an internal standard. Samples were vacuum dried, and reconstituted in 20% acetonitrile containing 250 µM caffeine as an additional internal standard. Resting cell samples were reconstituted in 225 µl reconstitution buffer, doubling the respective concentration of small molecules in comparison to the original sample. Lysate samples were reconstituted in 187.5µl, concentration in comparison to the original culture remained constant.

Samples were measured on a Q Exactive Plus-Orbitrap Mass Spectrometer (Thermo Fisher Scientific) in positive mode using a Kinetex C18 column (30 x 2.1 mm, 2.6 µm, 100 Å) for LC kept at room temperature. Mobile phase A: 5 mM formic acid in water:acetonitrile 98:2 (v/v); Mobile Phase B: 5 mM formic acid in water:acetonitrile 2:98 (v/v). 5 µl of

sample was injected at 95% mobile phase A, maintained for 3 minutes, followed by a linear gradient up to 98% B in 20 minutes, maintained for 7 minutes, followed by a linear gradient up to 95% A over 1 minute, which was maintained for 3 minutes. The flow rate was 0.3 ml/min. Samples were injected in three rounds representing three technical replicates including one washing injection every ten injections. Scan mode was FTMS + p ESI Full ms and scan range was from 60-800 *m/z*. Resolution was set to 70,000, AGC target to 1,000,000 ions, maximum IT to 150 ms. For secondary MS resolution was set to 17,500, AGC target to 100,000 ions, and maximum IT to 60 ms, allowing 5 secondary scans ranging from 200-2000 *m/z* per full scan at a collision energy of 35 eV. Unknown charges or charges higher than 2 were excluded from analysis. Ions with small fold changes were filtered out as described previously[51].

Raw data was converted from ThermoFisher .raw format into the open mzXML format using RawConverter[52]. For feature selection, peak alignment, grouping and retention time shift correction from the raw data the XCMS R package was used [53 54]. Parameters for first round of density grouping of peaks were bw=30, minfrac=0.5, minsamp=3, mzwid=0.025, max=50. For retention time correction, parameters were family="symmetric", plottype="mdevden". For second round of grouping, parameters were bw=10, minfrac=0.5, minsamp=3, mzwid=0.025, max=50. Missing peaks were filled using the “chrom” method. Statistical analysis was based on three biological replicates with two technical replicates each. Statistical analysis was based on [55,56]. Mapping to databases METLIN[57] and KEGG[58] were based on 10 ppm accuracy. Only H+ and ACN+H+ adducts were considered. For comparison between samples, all features were normalized using amitriptyline internal standard (*m/z* 278.18). For three of the metabolites, MS/MS matches to METLIN or internal database were used as additional annotation support (Supplementary Fig. 6c).

C. saccharolyticum secreted metabolite validation (Reverse phase LC-MS/MS, Q-ToF)

Bacterial cells were cultivated and treated with duloxetine as in the previous section. Cells were centrifuged (14000 rpm, 10 min, 4 °C) and 900 µl of the supernatant was extracted with 2700 µL ice-cold 1:1 methanol:acetonitrile. Following centrifugation (14000 rpm, 10 min, 4 °C), 3500 µL of the extracted metabolites were dried under vacuum (Savant DNA 120 SpeedVac concentrator, Thermo Scientific, with the following options: medium drying rate and heat option inactivated). Samples were reconstituted in 150 µL of 20% acetonitrile containing 10 µg/mL caffeine as an internal standard. Analytical standards for selected metabolites (xanthine, inosine, guanosine, adenosine and hypoxanthine) were reconstituted in 150 µL of 20% acetonitrile at a final concentration of 10 µg/mL.

Chromatographic separation was achieved using an Agilent Zorbax SB-C18 column (2.1 mm x 100 mm, 1.8-Micron) attached to an Agilent 1290 Infinity LC system coupled to Agilent 6546 LC/Q-TOF.

Column temperature was maintained at 40 °C. Mobile phase A consisted of 5 mM ammonium formate in water with 0.1% formic acid, and mobile phase B consisted of 5 mM ammonium formate in methanol with 0.1% formic acid. One µL of sample was injected at 95% mobile phase A, followed by a linear gradient up to 30% mobile phase B over one minute, followed by a linear gradient up to 100% mobile phase B over 7 minutes, which was

maintained for one minute. Post-run equilibration was achieved over 4 minutes. The flow rate was 0.2 mL/min.

The Agilent 6546 LC/Q-TOF was operated with the following source parameters: gas temperature, 200 °C; gas flow 9 l/min; nebulizer 35 psig; sheath gas temperature 400 oC; sheath gas flow 12 l/min; Vcap 2500 V; nozzle voltage 0 V; fragmentor 120 V; skimmer1 45 V; octupole RF peak 750. The instrument was operated in negative mode with the selection of the targeted MS/MS option for the following m/z: 151.0261 (xanthine, [M-H]-), 267.0734 (inosine, [M-H]-), 282.0841 (guanosine, [M-H]-), 266.089 (adenosine, [M-H]-) and 135.0312 (hypoxanthine, [M-H]-). The isolation width was set to medium (~4 amu), the collision energy to 10 eV and the acquisition time to 200 ms/spectra. The m/z range for MS and MS/MS was set to 50 - 500. Online mass calibration was performed using a second ionization source and a constant flow (2 ml/min) of reference solution (119.0363 and 1033.9881 m/z). For data analysis, the MassHunter Qualitative Analysis Software (Agilent, version 10.0) was utilized. Metabolite identification of xanthine, inosine, guanosine, and hypoxanthine in samples was performed by matching the retention time, the precursor m/z and the fragment ions m/z with the ones from the respective analytical standards (Supplementary Table 11).

Secreted metabolite analysis (flow-injection MS, Orbitrap)

Untargeted metabolomics analysis was performed as described previously[59,60]. Briefly, samples were analyzed on a platform consisting of a Thermo Scientific Ultimate 3000 liquid chromatography system with autosampler temperature set to 10 °C coupled to a Thermo Fisher Scientific Q-Exactive Plus Fourier transform mass spectrometer equipped with a heated electrospray ion source and operated in negative ionization mode. The isocratic flow rate was 150 µL/min of mobile phase consisting of 60:40% (v/v) isopropanol:water buffered with 1 mM ammonium fluoride at pH 9 and containing 10 nM taurocholic acid and 20 nM homotaurine as lock masses. Mass spectra were recorded in profile mode from 50 to 1,000 *m/z* with the following instrument settings: sheath gas, 35 a.u.; aux gas, 10 a.u.; aux gas heater, 200 °C; sweep gas, 1 a.u.; spray voltage, -3 kV; capillary temperature, 250 °C; S-lens RF level, 50 a.u; resolution, 70k @ 200 *m/z*; AGC target, $3x10^6$ ions, max. inject time, 120 ms; acquisition duration, 60 s. Spectral data processing was performed using an automated pipeline in R as described previously[59]. Detected ions were tentatively annotated as metabolites based on matching accurate mass within a tolerance of 5 mDa using the Human Metabolome database[61] as reference.

Secreted metabolite analysis (Hydrophilic interaction (HILIC) LC-MS and MS/MS, Q-ToF)

Liquid samples were prepared for LC-MS and LC-MS/MS analysis through the addition of an equal volume of ice cold (90:10) acetonitrile: 5 mM ammonium acetate (pH 9). Extractions were incubated for one hour at -20 °C followed by centrifugation at 4500 RPM (2850 g) for 10 min at 4 °C. 20 µL of extraction supernatant were transferred to Nunc 96-well, V-shape plates, closed with temperature sensitive seals and stored at -80 °C until further analysis. Samples were analyzed as previously reported (Agilent application note - 5994-1492EN). In brief, chromatographic separation was achieved using an Agilent InfinityLab Poroshell 120 HILIC-Z column, 2.1 mm × 150 mm, 2.7 µm column and an

Agilent 1290 Infinity II LC system coupled to an Agilent 6550 qToF mass spectrometer. Column temperature was maintained at 45 °C and the following mobile phase were used: Mobile phase A: Ammonium acetate 5mM, pH 9, and 250 µM InfinityLab Deactivator and Mobile Phase B: Ammonium acetate in acetonitrile:water 85:15 (v/v) 5mM, pH, 9, and 250 µM InfinityLab Deactivator (Agilent). 5 µL of sample were injected at 96% mobile phase B, maintained for 2 mins, followed by a linear gradient up to 88% B in 3.5 min, maintained for 3 min, followed by a linear gradient to 86% B in 0.5 min and maintained at 86% for 5 min, then a linear gradient to 82% mobile phase B over 3 mins, and a linear gradient to 65% B over 5 mins, which was maintained for 1min. The column was allowed to re-equilibrate HILIC conditions for 8 min before each sample injection. The flow rate was 0.25 ml/min. The qToF was operated in negative scanning mode (60–1,600 *m/z*) with the following source parameters: VCap, 3,500 V; nozzle voltage, 0 V; gas temperature, 225 °C; drying gas 13 l/min; nebulizer, 35 psi; sheath gas temperature 350 °C; sheath gas flow 12 l/min, fragmentor, 125 V and skimmer, 45 V. Online mass calibration was performed using a second ionization source and a constant flow (10 µL/min) of reference mass solution (119.0363 and 1033.9881 *m/z*).

LC–MS/MS analysis was performed using the same chromatographic separation conditions and source parameters described above, but using an Agilent 6546 qToF mass spectrometer, allowing operation in auto-MS/MS mode with iterative selection of a preferred inclusion list of parent ions. Parent ions for tandem mass spectrometry analysis were selected from the LC-MS data described above using 20 ppm mass tolerance and 0.5 min retention time tolerance, iso width set to ‘narrow width’ and collision energy to 10, 20 and 40 eV.

The MassHunter Qualitative Analysis Software (Agilent Technologies, version 10.0) was used for both LC-MS and LC-MS/MS molecular feature extraction. The following setting were applied: peak filter of absolute height: 5000 counts, limit assigned charge states to 1, only H-charged molecules were included and compound quality score cut-off was set to be greater than 80%. Peak alignment was carried out using Mass Profiler Professional (Agilent, version 15.1) with default parameters: mass tolerance of 2 mDa or 20 ppm and retention time tolerance of 0.3 min or 2%. A standard organic molecule model (MassHunter version 10.0, Agilent) was used to deisotope compounds and features were only extracted when at least two matching isotopes (retention time and relative abundance) could be detected. Only [M-H]-ions were considered for annotations. Extracted and aligned compounds were putatively annotated using the Metlin PCDL B.08.0 metabolite and peptide database/library, by using mass tolerance of 20 ppm.

For putative metabolite identification, cosine spectral similarity was computed for all the available collision energies using the SpectrumSimilarity function using OrgMassSpecR-v0.5-3 (cran.stat.upd.edu.ph/web/packages/OrgMassSpecR/). m/z tolerance for alignment was set to default (0.25). When multiple collision energies were available (both reference and measured), the one showing the highest spectral similarity score was retained. Molecules showing similarity score above 0.5 were assigned Metabolomics Standards Initiative (MSI)[62] ID level 2; molecules showing a spectral similarity score below 0.5 were assigned MSI ID level 3. MSI ID level 2 matches are shown in Supplementary Fig. 2. MSI level 1 assignment was made for linolenic acid and glycocholic acid based on

accurate mass and retention time comparison with chemical standards (Supplementary Fig. 3, Supplementary Table 17).

Cross-feeding candidate ion identification

Ions (*m/z* features) that were: i) not present in the starting medium, ii) increased during *S. salivarius* growth in the presence of duloxetine and, iii) decreased during *E. rectale* growth, were chosen as hits. Ions showing these characteristics in the DMSO (solvent) control were filtered out.

Community assembly assay

Overnight anaerobic cultures of the five bacterial species were inoculated in 2 ml GMM with 50 μM duloxetine to initial total cell concentration corresponding to OD of 0.1. Roughly equal amounts, by OD, were used from each of the five monocultures. Tubes were incubated for 48 h anaerobically at 37 °C without shaking. For DNA extraction, 1 mL of culture was centrifuged for 10 min 14.000 rpm in 1.5 mL eppendorf tubes. The bacterial pellet was frozen at -80 °C until DNA extraction. For drug extraction 600 μl of cold ACN:MethOH was added to the supernatant and incubated for 15 min in the fridge. Samples were then centrifuged for 10 min 14.000 rpm 4 °C, and 700 μl was transferred to a new tube and dried in a speedvac (Eppendorf Vacuum Concentrator Plus) for 5 h at 30 °C at V-AL mode. For UPLC measurement, the samples were reconstituted in 116 μl 20% ACN containing 250 μM caffeine as an internal standard.

DNA extraction and 16S barcode sequencing library preparation: Bacteria pellets were dissolved in lysis buffer and transferred into a 96 Polypropylene Deep Well plate (3959, Corning). An in-house protocol was used for DNA extraction. Specifically, the GNOME DNA isolation Kit (MP Biomedicals) was adapted to be used with the Biomek® FXp Liquid Handling Automation Workstation (Beckman). Subsequently, purified DNA was obtained using ZR-96 DNA Clean & ConcentratorTM-5 (D4024, Zymo Research). After the integrity of the DNA was verified by agarose gel electrophoresis, DNA concentration of the samples was determined using the Qubit dsDNA BR assay kit (Q32850, life technologies) in combination with the Infinite® M1000 PRO plate reader (Tecan). The 16S V4 amplicons were generated using an Illumina-compatible 2-step PCR protocol: in the first PCR the 16S V4 region was amplified with the primers F515/R806[63] and then in the second PCR barcode sequences were introduced using the NEXTflex 16S V4 Amplicon-Seq Kit (4201-05, Bioo Scientific). After multiplexing equal volumes of PCR products from each sample, SPRIselect reagent kit (B23318, Beckman Coulter) was used for left-side size selection. Prior to Illumina sequencing, the quality of the library was checked by the 2100 BioAnalyzer (Agilent Technologies) and the DNA concentration was determined using the Qubit dsDNA HS assay kit. Sequencing was performed using a 250 bp paired-end sequencing protocol on the Illumina MiSeq platform (Illumina, San Diego, USA) at the Genomics Core Facility (EMBL Heidelberg).

16S barcode sequencing analysis: The raw Illumina paired-end reads were quality trimmed and length filtered using CUTADAPT with quality threshold of 30 bp and length cutoff of 150 bp. The amplicon sequences were compared to the 16S rRNA gene of the species mixed

Europe PMC Funders Author Manuscripts

for coculture using UCLUST[64]. Only those that have minimum 98% identity were clustered into the operational taxonomic units (OTUs). The species abundance was normalized by the 16S rRNA gene copy numbers.

Conditioned Media Assay

The supernatant of cultures of *S. salivarius* treated with 50 μM duloxetine or equivalent amount of DMSO (solvent control) were filtered with a Millipore 0.22 μm filter after centrifugation. To additionally account for the duloxetine's impact on bacterial growth, duloxetine was added to the supernatant from the untreated control to 50 μM concentration. The resulting conditioned media or spent media control were inoculated with *E. rectale* at OD^{578} of 0.01 and the growth was measured by following OD. Experiments were performed in triplicates.

C. elegans duloxetine interaction assays

Bacteria were incubated with duloxetine as follows: 0.5 ml of overnight bacterial culture (or LB only for controls) was added to 4.5 ml LB and shaken for 2 h at 37 °C, after which duloxetine was added and shaking continued for a further 22 h. Cultures were centrifuged at 4,500 rpm for 10 min and supernatant was sterilized by passing through a 0.22 μm filter. *C. elegans* N2 wild type (WT) was maintained in nematode growth media (NGM), as previously described[65]. Worms at the L4 larval stage raised on NGM plates containing *E. coli* BW25113 bacteria were washed thrice in M9. 50 animals per 100 μl of control LB media with DMSO, LB media with duloxetine at 0, 0.1, 0.5 and 1 mM or spent LB media from *E. coli* IAI1 or ED1a were added to a 96-well flat-bottom microtiter plate. Assay plates were incubated at 20 °C for 60 min, with regular shaking at 140 rpm and the number of regular moving animals (displaying movement at least once every 3 seconds) were counted and expressed as a percentage of total worms per well.

Replicates and statistical tests

Technical replicates refer to replicates within the same batch (e.g. three bacterial cultures inoculated from the same starting culture), while biological replicates refer to independent experiments. All indicated sample numbers (or displayed data points) refer to distinct samples (biological replicates) and not to repeated measurements of the same samples. All statistical tests are two-sided. FDR corrections were performed using Benjamini-Hochberg procedure.

Supplementary Material

Refer to Web version on PubMed Central for supplementary material.

Acknowledgements

This project was supported by European Union's Horizon 2020 research and innovation programme under the grant agreement number 686070, and by the UK Medical Research Council (project number MC_UU_00025/11). A.M., L.M., M.T. and V.P. were supported by EMBL interdisciplinary postdoctoral program. We thank EMBL Genomics, Metabolomics and Proteomics core facilities for their support in respective analyses.

Data availability

All data generated during this study are included in this published article (and its supplementary information files). Suppl. Table 18 provides overview of the different methods and data associated with all figures. UPLC and mass-spectrometry data are deposited at the MetaboLights repository under the accession codes MTBLS1264 (ebi.ac.uk/metabolights/MTBLS1264), MTBLS1757 (ebi.ac.uk/metabolights/MTBLS1757), MTBLS1627 (ebi.ac.uk/metabolights/MTBLS1627), MTBLS1319 (ebi.ac.uk/metabolights/MTBLS1319), MTBLS1791 (ebi.ac.uk/metabolights/MTBLS1791), MTBLS1792 (ebi.ac.uk/metabolights/MTBLS1792), and MTBLS2885 (ebi.ac.uk/metabolights/MTBLS2885). The mass spectrometry proteomics data have been deposited to the ProteomeXchange Consortium with the dataset identifiers PXD016062 (ebi.ac.uk/pride/archive/projects/PXD016062) and PXD016064 (ebi.ac.uk/pride/archive/projects/PXD016064).

Code availability

The data analysis codes are available at github.com/sandrejev/drugs_bioaccumulation.

References

1. Zimmermann M, Zimmermann-Kogadeeva M, Wegmann R, Goodman AL. Mapping human microbiome drug metabolism by gut bacteria and their genes. Nature. 2019; 570: 462. doi: 10.1038/s41586-019-1291-3 [PubMed: 31158845]
2. Forslund K, Hildebrand F, Nielsen T, Falony G. Disentangling type 2 diabetes and metformin treatment signatures in the human gut microbiota. Nature. 2015; 528: 262–266. DOI: 10.1038/nature15766 [PubMed: 26633628]
3. Falony G, et al. Population-level analysis of gut microbiome variation. Science. 2016; 352: 560–564. DOI: 10.1126/science.aad3503 [PubMed: 27126039]
4. Maier L, Typas A. Systematically investigating the impact of medication on the gut microbiome. Curr Opin Microbiol. 2017; 39: 128–135. DOI: 10.1016/j.mib.2017.11.001 [PubMed: 29169088]
5. Jackson MA, et al. Gut microbiota associations with common diseases and prescription medications in a population-based cohort. Nat Commun. 2018; 9 doi: 10.1038/s41467-018-05184-7
6. Maier L, et al. Extensive impact of non-antibiotic drugs on human gut bacteria. Nature. 2018; doi: 10.1038/nature25979
7. Spanogiannopoulos P, Bess EN, Carmody RN, Turnbaugh PJ. The microbial pharmacists within us: a metagenomic view of xenobiotic metabolism. Nature Reviews Microbiology. 2016; 14: 273–287. DOI: 10.1038/nrmicro.2016.17 [PubMed: 26972811]
8. Alexander JL, et al. Gut microbiota modulation of chemotherapy efficacy and toxicity. Nat Rev Gastroenterol Hepatol. 2017; 14: 356–365. DOI: 10.1038/nrgastro.2017.20 [PubMed: 28270698]
9. Fuller AT. Is p-aminobenzenesulphonamide the active agent in prontosil therapy? The Lancet. 1937; 229: 194–198. DOI: 10.1016/S0140-6736(00)97447-6
10. Goldman P, Peppercorn MA, Goldin BR. Metabolism of drugs by microorganisms in the intestine. Am J Clin Nutr. 1974; 27: 1348–1355. [PubMed: 4155602]
11. Chhabra RS. Intestinal absorption and metabolism of xenobiotics. Environ Health Perspect. 1979; 33: 61–69. [PubMed: 540626]
12. Koppel N, Maini Rekdal V, Balskus EP. Chemical transformation of xenobiotics by the human gut microbiota. Science. 2017; 356 doi: 10.1126/science.aag2770
13. Sousa T, et al. The gastrointestinal microbiota as a site for the biotransformation of drugs. Int J Pharm. 2008; 363: 1–25. DOI: 10.1016/j.ijpharm.2008.07.009 [PubMed: 18682282]

14. Klaassen CD, Cui JY. Review: Mechanisms of How the Intestinal Microbiota Alters the Effects of Drugs and Bile Acids. Drug Metab Disp. 2015; 43: 1505–1521. DOI: 10.1124/dmd.115.065698
15. Haiser HJ, Seim KL, Balskus EP, Turnbaugh PJ. Mechanistic insight into digoxin inactivation by Eggerthella lenta augments our understanding of its pharmacokinetics. Gut microbes. 2014; 5: 233–238. [PubMed: 24637603]
16. Koppel N, Bisanz JE, Pandelia M-E, Turnbaugh PJ, Balskus EP. Discovery and characterization of a prevalent human gut bacterial enzyme sufficient for the inactivation of a family of plant toxins. Elife. 2018; 7 e33953 doi: 10.7554/eLife.33953 [PubMed: 29761785]
17. Wallace BD, Wang H, Lane KT, Scott JE. Alleviating cancer drug toxicity by inhibiting a bacterial enzyme. Science. 2010; 330: 831–835. DOI: 10.1126/science.1191175 [PubMed: 21051639]
18. Tramontano M, et al. Nutritional preferences of human gut bacteria reveal their metabolic idiosyncrasies. Nat Microbiol. 2018; doi: 10.1038/s41564-018-0123-9
19. Chrystal EJT, Koch RL, McLafferty MA, Goldman P. Relationship between metronidazole metabolism and bactericidal activity. Antimicrobial Agents and Chemotherapy. 1980; 18: 566–573. DOI: 10.1128/AAC.18.4.566 [PubMed: 6255861]
20. Mahmood S, Khalid A, Arshad M, Mahmood T, Crowley DE. Detoxification of azo dyes by bacterial oxidoreductase enzymes. Critical Reviews in Biotechnology. 2015; 36: 1–13. DOI: 10.3109/07388551.2015.1004518
21. Khan AKA, Guthrie G, Johnston HH, Truelove SC, Williamson DH. Tissue and Bacterial Splitting of Sulphasalazine. Clinical Science. 1983; 64: 349–354. DOI: 10.1042/cs0640349 [PubMed: 6129936]
22. Goodman AL, et al. Extensive personal human gut microbiota culture collections characterized and manipulated in gnotobiotic mice. P Natl Acad Sci USA. 2011; 108: 6252–6257. DOI: 10.1073/pnas.1102938108
23. Shu YZ, Kingston DG. Metabolism of levamisole, an anti-colon cancer drug, by human intestinal bacteria. Xenobiotica. 1991; 21: 737–750. DOI: 10.3109/00498259109039513 [PubMed: 1949905]
24. Schloissnig S, et al. Genomic variation landscape of the human gut microbiome. Nature. 2013; 493: 45–50. DOI: 10.1038/nature11711 [PubMed: 23222524]
25. Fenner K, Canonica S, Wackett LP, Elsner M. Evaluating pesticide degradation in the environment: blind spots and emerging opportunities. Science. 2013; 341: 752–758. DOI: 10.1126/science.1236281 [PubMed: 23950532]
26. Gulde R, Anliker S, Kohler HE, Fenner K. Ion Trapping of Amines in Protozoa: A Novel Removal Mechanism for Micropollutants in Activated Sludge. Environ Sci Technol. 2018; 52: 52–60. DOI: 10.1021/acs.est.7b03556 [PubMed: 29182849]
27. Congeevaram S, Dhanarani S, Park J, Dexilin M, Thamaraiselvi K. Biosorption of chromium and nickel by heavy metal resistant fungal and bacterial isolates. J Hazard Mater. 2007; 146: 270–277. DOI: 10.1016/j.jhazmat.2006.12.017 [PubMed: 17218056]
28. Bae W, Chen W, Mulchandani A, Mehra RK. Enhanced bioaccumulation of heavy metals by bacterial cells displaying synthetic phytochelatins. Biotechnol Bioeng. 2000; 70: 518–524. DOI: 10.1002/1097-0290(20001205)70:5<518::aid-bit6>3.0.co;2-5 [PubMed: 11042548]
29. Becher I, et al. Thermal profiling reveals phenylalanine hydroxylase as an off-target of panobinostat. Nat Chem Biol. 2016; 12: 908–910. DOI: 10.1038/nchembio.2185 [PubMed: 27669419]
30. Franken H, et al. Thermal proteome profiling for unbiased identification of direct and indirect drug targets using multiplexed quantitative mass spectrometry. Nat Protoc. 2015; 10: 1567–1593. DOI: 10.1038/nprot.2015.101 [PubMed: 26379230]
31. Brochado AR, et al. Species-specific activity of antibacterial drug combinations. Nature. 2018; 559: 259–263. DOI: 10.1038/s41586-018-0278-9 [PubMed: 29973719]
32. Rakoff-Nahoum S, Coyne MJ, Comstock LE. An Ecological Network of Polysaccharide Utilization Among Human. Curr Biol. 2014; 24: 40–49. [PubMed: 24332541]
33. Hooper LV, Littman DR, Macpherson AJ. Interactions between the microbiota and the immune system. Science. 2012; 336: 1268–1273. DOI: 10.1126/science.1223490 [PubMed: 22674334]

Europe PMC Funders Author Manuscripts

34. Zhang F, et al. Caenorhabditis elegans as a Model for Microbiome Research. Front Microbiol. 2017; 8: 485. doi: 10.3389/fmicb.2017.00485 [PubMed: 28386252]
35. Vetizou M, et al. Anticancer immunotherapy by CTLA-4 blockade relies on the gut microbiota. Science. 2015; 350: 1079. doi: 10.1126/science.aad1329 [PubMed: 26541610]
36. Wu H, et al. Metformin alters the gut microbiome of individuals with treatment-naive type 2 diabetes, contributing to the therapeutic effects of the drug. Nature Medicine. 2017; doi: 10.1038/nm.4345
37. Macedo D, et al. Antidepressants, antimicrobials or both? Gut microbiota dysbiosis in depression and possible implications of the antimicrobial effects of antidepressant drugs for antidepressant effectiveness. Journal of Affective Disorders. 2017; 208: 22–32. DOI: 10.1016/j.jad.2016.09.012 [PubMed: 27744123]
38. Sharon G, Sampson TR, Geschwind DH, Mazmanian SK. The Central Nervous System and the Gut Microbiome. Cell. 2016; 167: 915–932. DOI: 10.1016/j.cell.2016.10.027 [PubMed: 27814521]
39. Dent R, et al. Changes in body weight and psychotropic drugs: a systematic synthesis of the literature. PLoS One. 2012; 7 e36889 doi: 10.1371/journal.pone.0036889 [PubMed: 22719834]
40. Kanehisa M, et al. Data, information, knowledge and principle: back to metabolism in KEGG. Nucleic acids research. 2014; 42: D199–205. DOI: 10.1093/nar/gkt1076 [PubMed: 24214961]
41. Cox J, Mann M. MaxQuant enables high peptide identification rates, individualized p.p.b.-range mass accuracies and proteome-wide protein quantification. Nat Biotechnol. 2008; 26: 1367–1372. DOI: 10.1038/nbt.1511 [PubMed: 19029910]
42. Cox J, et al. Andromeda: A peptide search engine integrated into the MaxQuant environment. Journal of Proteome Research. 2011; 10: 1794–1805. DOI: 10.1021/pr101065j [PubMed: 21254760]
43. Elias JE, Gygi SP. Target-decoy search strategy for increased confidence in large-scale protein identifications by mass spectrometry. Nat Methods. 2007; 4: 207–214. DOI: 10.1038/nmeth1019 [PubMed: 17327847]
44. Gentleman RC, et al. Bioconductor: open software development for computational biology and bioinformatics. Genome Biology. 2004; 5: R80. doi: 10.1186/gb-2004-5-10-r80 [PubMed: 15461798]
45. Benjamini Y, Hochberg Y. Controlling the False Discovery Rate: A Practical and Powerful Approach to Multiple Testing. Journal of the Royal Statistical Society Series B (Methodological). 1995; 57: 289–300. DOI: 10.2307/2346101
46. Conesa A, et al. Blast2GO: A universal tool for annotation, visualization and analysis in functional genomics research. Bioinformatics. 2005; 21: 3674–3676. DOI: 10.1093/bioinformatics/bti610 [PubMed: 16081474]
47. Porollo A. EC2KEGG: a command line tool for comparison of metabolic pathways. Source code for biology and medicine. 2014; 9: 19. doi: 10.1186/1751-0473-9-19 [PubMed: 25202338]
48. Mateus A, et al. Thermal proteome profiling in bacteria: probing protein state in vivo. Mol Syst Biol. 2018; 14 e8242 doi: 10.15252/msb.20188242 [PubMed: 29980614]
49. Hughes CS, et al. Ultrasensitive proteome analysis using paramagnetic bead technology. Mol Syst Biol. 2014; 10: 757. doi: 10.15252/msb.20145625 [PubMed: 25358341]
50. Hughes CS, et al. Single-pot, solid-phase-enhanced sample preparation for proteomics experiments. Nat Protoc. 2019; 14: 68–85. DOI: 10.1038/s41596-018-0082-x [PubMed: 30464214]
51. Ortmayr K, Charwat V, Kasper C, Hann S, Koellensperger G. Uncertainty budgeting in fold change determination and implications for non-targeted metabolomics studies in model systems. The Analyst. 2016; doi: 10.1039/C6AN01342B
52. He L, Diedrich J, Chu YY, Yates JR 3rd. Extracting Accurate Precursor Information for Tandem Mass Spectra by RawConverter. Anal Chem. 2015; 87: 11361–11367. DOI: 10.1021/acs.analchem.5b02721 [PubMed: 26499134]
53. Mahieu NG, Genenbacher JL, Patti GJ. A roadmap for the XCMS family of software solutions in metabolomics. Curr Opin Chem Biol. 2016; 30: 87–93. DOI: 10.1016/j.cbpa.2015.11.009 [PubMed: 26673825]

54. Smith CA, Want EJ, O'Maille G, Abagyan R, Siuzdak G. XCMS: processing mass spectrometry data for metabolite profiling using nonlinear peak alignment, matching, and identification. Anal Chem. 2006; 78: 779–787. DOI: 10.1021/ac051437y [PubMed: 16448051]
55. Ortmayr K, Charwat V, Kasper C, Hann S, Koellensperger G. Uncertainty budgeting in fold change determination and implications for non-targeted metabolomics studies in model systems. Analyst. 2016; 142: 80–90. DOI: 10.1039/c6an01342b [PubMed: 27722392]
56. Vinaixa M, et al. A Guideline to Univariate Statistical Analysis for LC/MS-Based Untargeted Metabolomics-Derived Data. Metabolites. 2012; 2: 775–795. DOI: 10.3390/metabo2040775 [PubMed: 24957762]
57. Smith CA, et al. METLIN: a metabolite mass spectral database. Ther Drug Monit. 2005; 27: 747–751. DOI: 10.1097/01.ftd.0000179845.53213.39 [PubMed: 16404815]
58. Tanabe M, Kanehisa M. Using the KEGG database resource. Current protocols in bioinformatics / editoral board, Andreas D Baxevanis. 2012; doi: 10.1002/0471250953.bi0112s38
59. Fuhrer T, Heer D, Begemann B, Zamboni N. High-throughput, accurate mass metabolome profiling of cellular extracts by flow injection–time-of-flight mass spectrometry. Analytical chemistry. 2011; 83: 7074–7080. [PubMed: 21830798]
60. Ponomarova O, et al. Yeast Creates a Niche for Symbiotic Lactic Acid Bacteria through Nitrogen Overflow. Cell Syst. 2017; 5: 345–357. e346 doi: 10.1016/j.cels.2017.09.002 [PubMed: 28964698]
61. Wishart DS, et al. HMDB 4.0: the human metabolome database for 2018. Nucleic Acids Res. 2018; 46: D608–D617. DOI: 10.1093/nar/gkx1089 [PubMed: 29140435]
62. Sumner LW, et al. Proposed minimum reporting standards for chemical analysis Chemical Analysis Working Group (CAWG) Metabolomics Standards Initiative (MSI). Metabolomics. 2007; 3: 211–221. DOI: 10.1007/s11306-007-0082-2 [PubMed: 24039616]
63. Caporaso JG, et al. Global patterns of 16S rRNA diversity at a depth of millions of sequences per sample. P Natl Acad Sci USA. 2011; 108: 4516–4522. DOI: 10.1073/pnas.1000080107
64. Edgar RC. Search and clustering orders of magnitude faster than BLAST. Bioinformatics. 2010; 26: 2460–2461. DOI: 10.1093/bioinformatics/btq461 [PubMed: 20709691]
65. Brenner S. The genetics of Caenorhabditis elegans. Genetics. 1974; 77: 71–94. [PubMed: 4366476]

Europe PMC Funders Author Manuscripts

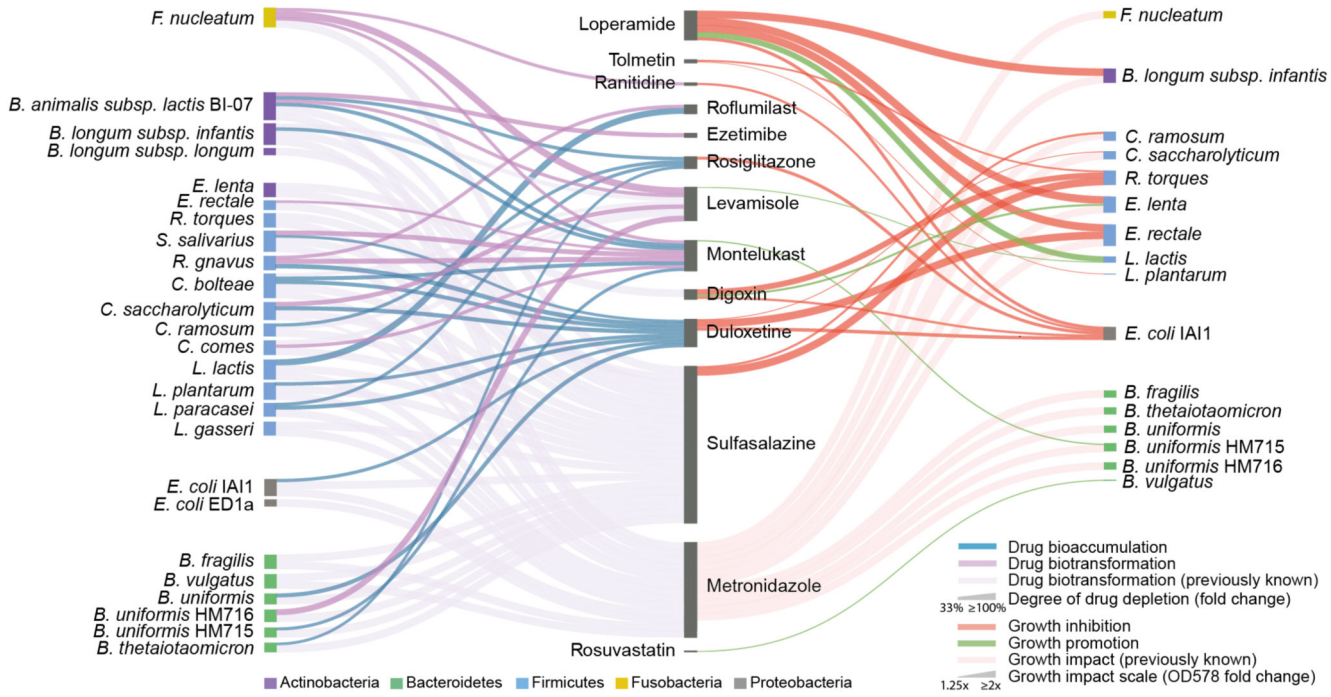

Fig 1. Gut bacteria accumulate therapeutic drugs without altering them.

Bacteria-drug interaction network identified in our study (see main text). Left network: Biotransformation or bioaccumulation of drugs by gut bacteria. Shown are the interactions significant in two independent screens, and validated in a follow-up assay (Wilcoxon's rank sum test, FDR corrected $p < 0.05$). Also included are previously reported interactions that were detected in the screen but not tested in the validation assay. Right network: Growth impact of drugs on gut bacteria as detected in at least two independent screens. (Student's t-test, alpha=0.05).

Europe PMC Funders Author Manuscripts

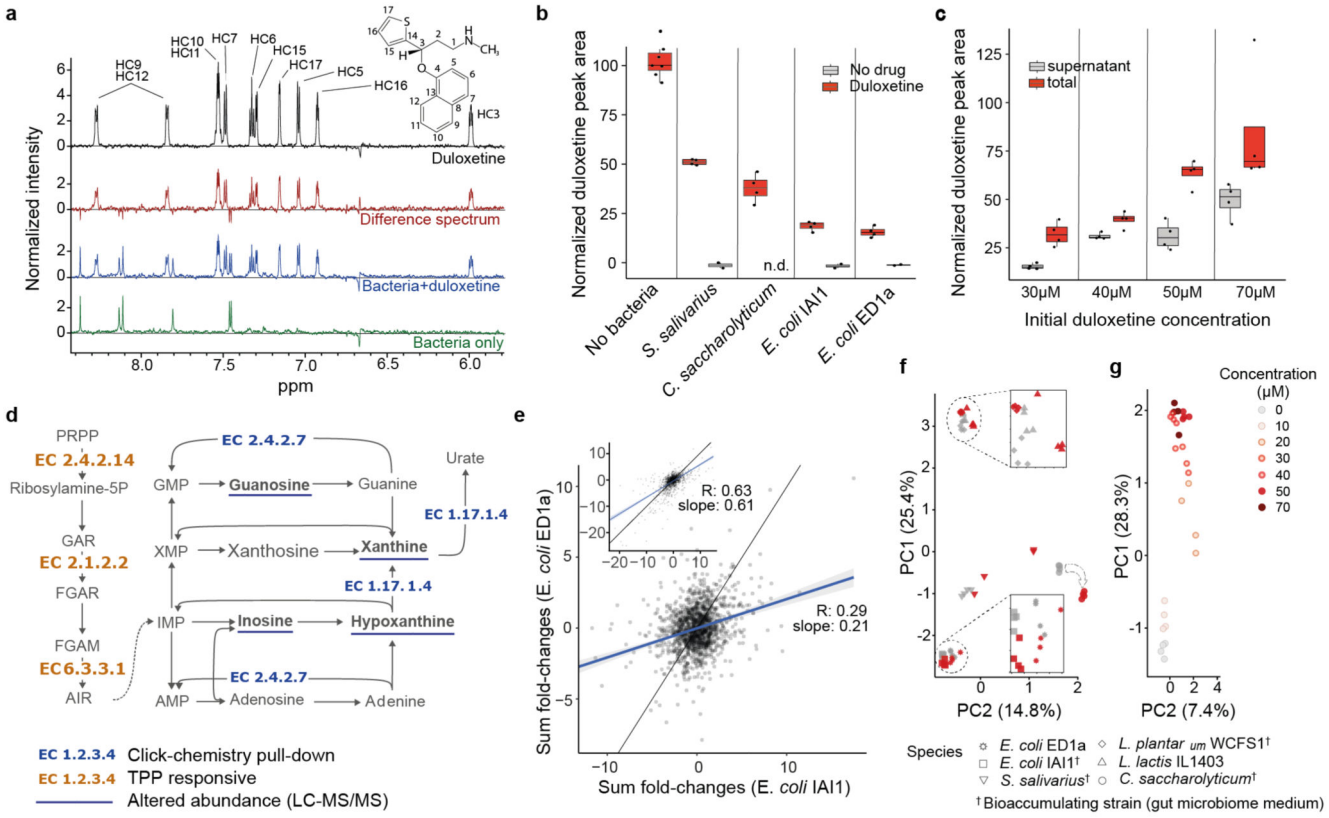

Fig 2. Bioaccumulation of duloxetine impacts bacterial physiology.

a) NMR analysis showing bioaccumulation of duloxetine by *S. salivarius*. Drug measurements in cell-free supernatant. Differential spectrum contrasts the drug-treated and untreated cells. **b)** NMR quantification of duloxetine in the supernatants of three gut bacterial strains treated with 50 μM duloxetine. n=4 biologically independent replicates for drug treatment, n=2 technical replicates for drug-free controls, n=7 biologically independent replicates for bacteria-free controls. n.d. = no peak detected. Bioaccumulation assays in (**a, b**) performed in PBS buffer. **c)** LC-MS quantification of duloxetine in *C. saccharolyticum* bioaccumulation assays in GMM at different initial drug concentrations (n=4 biologically independent replicates). Boxplots in (**b, c**) show the interquartile range (IQR), the median, and whiskers extending to 1.5 × IQR from the 1st or 3rd quartile. **d)** *C. saccharolyticum* nucleotide biosynthetic pathway marking the duloxetine-binding or responding enzymes (EC numbers shown) and the differentially secreted metabolites (underlined). **e)** *E. coli* IAI1 (bioaccumulating in GMM) and *E. coli* ED1a (non-bioaccumulating in GMM) strains respond differentially to duloxetine in thermal proteome profiling (TPP) analysis. Each dot represents the summed log2 fold-changes across all temperatures for an identified protein. Main panel: duloxetine added to intact cells prior to TPP (1437 proteins in total); inset: TPP results when drug added to the cell lysates (1694 proteins in total). The black line marks the diagonal, and the blue line shows the linear regression fit. Error bands around the blue lines show 95% confidence interval. Data for both intact cells and lysate TPP is based on n=5 independent experiments for each strain (4 different drug concentrations and a vehicle control). **f)** Impact of duloxetine treatment on the exo-metabolome (untargeted

Europe PMC Funders Author Manuscripts

HILIC-MS, Methods) of six gut bacterial strains. The numbers in parentheses mark the explained variance for the corresponding principal components. The dotted arrow marks the duloxetine induced shift in the exo-metabolome of *C. saccharolyticum*. **g)** Duloxetine induced changes in the *C. saccharolyticum* exo-metabolome are concentration dependent.

Europe PMC Funders Author Manuscripts

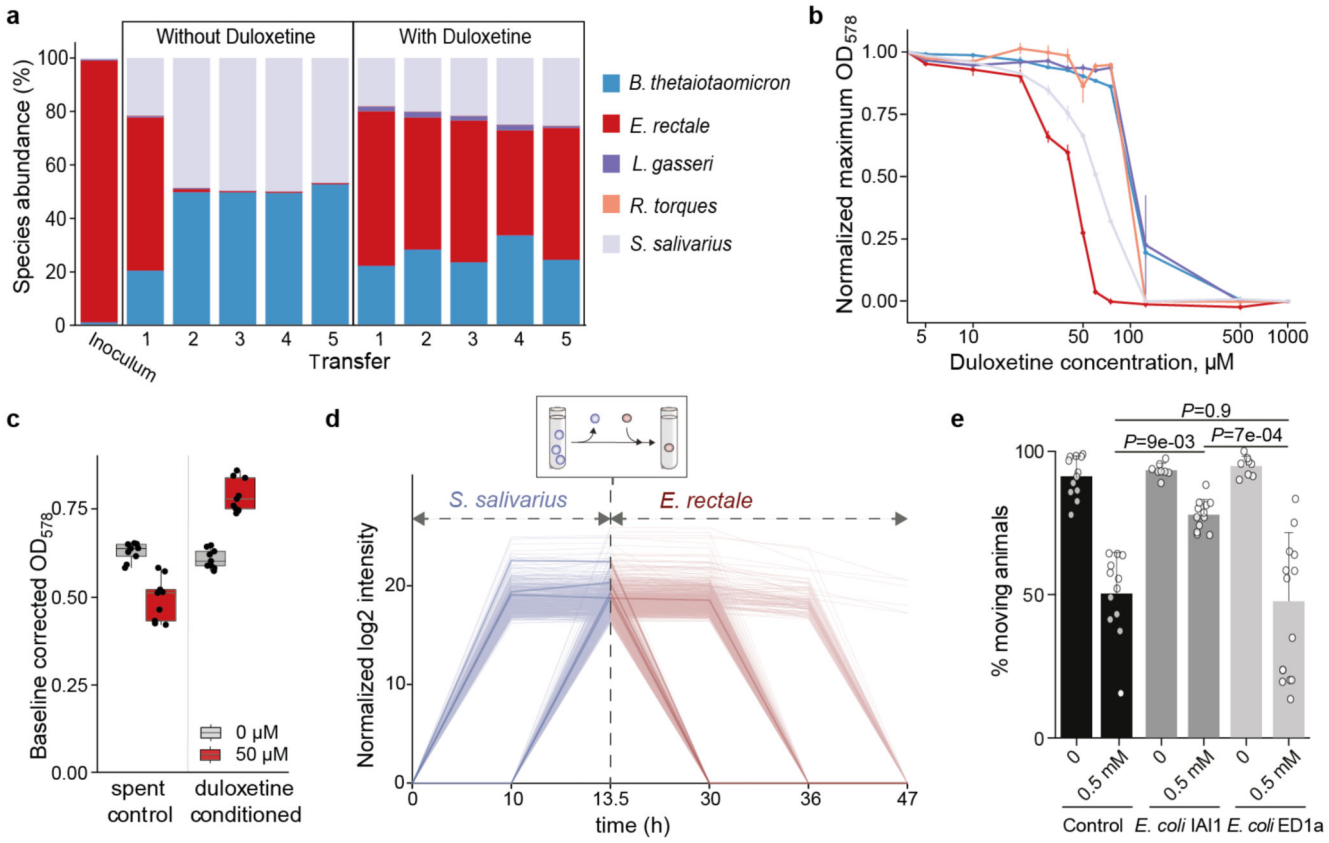

Fig 3. Duloxetine bioaccumulation alters community assembly and host response.

a) Community assembly is impacted by duloxetine. A starting mixture of five bacteria was transferred to fresh medium with or without duloxetine every 48 hours (Methods). Shown is the profile of mean relative abundances estimated using 16S rRNA amplicon sequencing (biological triplicates). Apparent initial uneven distribution is due to interspecies differences in cell lysis and gene amplification efficiency. The trend of *E. rectale* normalized to the inoculum signal in Supplementary Fig. 9b. **b)** Mono-culture duloxetine sensitivity of the five species used in (a). For each concentration-strain combination, n=3 independent growth curves. Error bars depict standard deviation, central circles mark the mean. **c)** OD578 of *E. rectale* grown on spent medium of *S salivarius*. Medium was supplemented with duloxetine either before (drug conditioned) or after (spent control) *S. salivarius* growth. n=9, three biological and three technical replicates. Boxplots show the interquartile range (IQR), the median, and whiskers extending to 1.5 × IQR from the 1st or 3rd quartile. **d)** Metabolite profiles (956 in total, untargeted HILIC-MS analysis, Methods) that increased during *S. salivarius* growth in GMM and decreased during *E. rectale* growth in the cell-free conditioned medium of *S. salivarius*, implying cross-feeding. Thicker lines mark 5 metabolites putatively assigned using HILIC-MS/MS, two of which (linolenic acid and glycocholic acid) were confirmed against analytical standards. Mean intensities from three biological replicates are shown. **e)** Percentage of worms displaying movement in spent LB media pre-incubated with 0.5 mM duloxetine in the absence or presence of *E. coli* IAI1 (bioaccumulating) or *E. coli* ED1a (non-bioaccumulating). n = 8 (column 3 and 5;

Europe PMC Funders Author Manuscripts

4 biological X 2 technical replicates) or 12 (all other columns; 6 biological X 2 technical replicates). Bar heights mark mean, error bars = standard deviation. P-values estimated using one-way ANOVA followed by correction for multiple pair-wise comparisons (Tukey's test). Duloxetine measurements in Supplementary Fig. 9f.

Europe PMC Funders Author Manuscripts